TITLE

Omics-Based Interaction Framework – a systems model to reveal molecular drivers of synergy

AUTHORS

Jezreel Pantaleón García[1], Vikram V. Kulkarni[1,2], Tanner C. Reese[1,3], Shradha Wali[1,2], Saima J. Wase[1], Jiexin Zhang[4], Ratnakar Singh[5,], Mauricio S. Caetano[1], Seyed Javad Moghaddam[1], Faye M. Johnson[5], Jing Wang[4], Yongxing Wang[1], Scott E. Evans[1,2]

[1] Department of Pulmonary Medicine, University of Texas MD Anderson Cancer Center, Houston, Texas, USA 77030

[2] MD Anderson Cancer Center UT Health Graduate School of Biomedical Sciences, Houston, Texas, USA 77030

[3] Rice University, Houston, Texas, USA, 77005

[4] Department of Bioinformatics and Computational Biology, University of Texas MD Anderson Cancer Center, Houston, Texas, USA 77030

[5] Department of Thoracic, Head and Neck Medical Oncology, University of Texas MD Anderson Cancer Center, Houston, Texas, USA 77030

CORRESPONDING AUTHOR: Scott E. Evans, MD
6565 MD Anderson Blvd, Unit 1059
Houston, TX, USA 77030
seevans@mdanderson.org
(Office) 713 – 563 – 7433

RUNNING TITLE: Omics-Based Systems Synergy Model

FINAL CHARACTER COUNT: 62850

ABSTRACT

Bioactive molecule library screening strategies may empirically identify effective combination therapies. However, without a systems theory to interrogate synergistic responses, the molecular mechanisms underlying favorable drug-drug interactions remain unclear, precluding rational design of combination therapies. Here, we introduce Omics-Based Interaction Framework (OBIF) to reveal molecular drivers of synergy through integration of statistical and biological interactions in supra-additive biological responses. OBIF performs full factorial analysis of feature expression data from single vs. dual factor exposures to identify molecular clusters that reveal synergy-mediating pathways, functions and regulators. As a practical demonstration, OBIF analyzed a therapeutic dyad of immunostimulatory small molecules that induces synergistic protection against influenza A pneumonia. OBIF analysis of transcriptomic and proteomic data identified biologically relevant, unanticipated cooperation between RelA and cJun that we subsequently confirmed to be required for the synergistic antiviral protection. To demonstrate generalizability, OBIF was applied to data from a diverse array of Omics platforms and experimental conditions, successfully identifying the molecular clusters driving their synergistic responses. Hence, OBIF is a phenotype-driven systems model that supports multiplatform exploration of synergy mechanisms.

KEYWORDS

Multi-Omics; Synergy; Data integration; Inducible epithelial resistance; Pneumonia

SUBJECT CATEGORIES

Genome-Scale and Integrative Biology; Methods & Resources; Microbiology, Virology & Host Pathogen Interaction

50 **INTRODUCTION**

51 Superior treatment outcomes are achieved for many disease states when more than one therapeutic
52 agent is administered (Chen *et al*, 2015; Zappasodi *et al*, 2018; Ronzitti *et al*, 2018; Han *et al*, 2019).
53 Indeed, there are many well documented instances when the therapeutic benefit of two agents
54 administered together substantially exceeds the benefit that would be predicted by the additive effects of
55 the agents administered individually. Widespread availability of high throughput technologies has allowed
56 multi-level study of complex biological responses from genome to phenome (Hasin *et al*, 2017). Yet, there
57 remains lack of consensus regarding the appropriate analysis of statistical and biological interactions
58 found in non-additive (i.e., antagonistic or synergistic) responses (Wei *et al*, 2018). Moreover, previously
59 proposed strategies to analyze non-additive interactions frequently lack sufficient generalizability to study
60 these processes outside of their home Omics platforms (Chen *et al*, 2015). Thus, while synergistic
61 therapeutic combinations may be empirically derived from fortuitous clinical experiences or through
62 screening of bioactive small molecule libraries, the absence of an established means to investigate these
63 favorable drug-drug interactions ultimately precludes understanding of their underlying mechanisms.
64 Consequently, development of a methodology to integrate the statistical and biological components of
65 synergistic interactions in diverse Omics settings can advance the rational design of combination
66 therapies while affording understanding of their molecular mechanisms against diseases.

67

68 Pneumonia is a major worldwide cause of death and frequently requires combination therapies (Troeger
69 *et al*, 2017; Metlay *et al*, 2019). We have previously reported that a therapeutic dyad of
70 immunostimulatory small molecules induces synergistic protection against a broad range of pneumonia-
71 causing pathogens (Duggan *et al*, 2011, Cleaver *et al*, 2014, Kirkpatrick *et al*, 2018; Ware *et al*, 2019).
72 This combination (hereafter, "Pam2-ODN") is comprised of a Toll-like receptor (TLR) 2/6 agonist,
73 Pam2CSK4 ("Pam2"), and a TLR 9 agonist, ODN M362 ("ODN"), that stimulate protective responses
74 from lung epithelial cells (Cleaver *et al*, 2014). This biological response, termed inducible epithelial

resistance, promotes survival benefits and microbicidal effects that significantly exceed the additive effects of the individual ligands (Duggan *et al*, 2011; Tuvim *et al*, 2012). Thus, understanding the molecular mechanisms underlying this unanticipated synergy may allow optimized manipulation of epithelial antimicrobial responses and support new generations of host-based therapeutics against infections.

In the absence of a systems theory to interrogate synergistic mechanisms (Wei *et al*, 2018), we introduce Omics-Based Interaction Framework (OBIF) to identify molecular drivers of synergy through integration of statistical and biological interactions in supra-additive biological responses. Unlike exploratory synergy models (Chen *et al*, 2015), OBIF is a phenotype-driven model (Hasin *et al*, 2017) that performs full factorial analysis (Li *et al*, 2009; Antony, 2014; Das *et al*, 2018) of feature expression data from single vs. dual factor exposures to identify molecular clusters that reveal synergy-mediating pathways, functions and regulators. To demonstrate the utility of OBIF, we applied this strategy to multi-Omics experimental data from epithelial cells exposed to Pam2-ODN to identify biologically relevant, unanticipated cooperative signaling events that we subsequently confirmed to be required for the synergistic pneumonia protection. Then, to demonstrate generalizability, OBIF was applied to datasets from diverse types of Omics platforms and experimental models, successfully identifying molecular clusters driving their synergistic responses.

RESULTS

Synergistic Pam2-ODN-inducible epithelial resistance against pneumonia

Our laboratory's interest in synergistic interactions arises from our experience investigating single vs. dual immunostimulatory treatments to prevent pneumonia (Duggan *et al*, 2011; Tuvim *et al*, 2012; Cleaver *et al*, 2014; Kirkpatrick *et al*, 2018; Ware *et al*, 2019). As a demonstrative example, data are presented here from influenza A virus (IAV) challenges of different models following pretreatment with

100 Pam2 alone, ODN alone or the Pam2-ODN combination. When mice are challenged with IAV 24 h after
101 the indicated inhaled treatments, we observed little increase in survival after the individual treatments
102 compared to sham-treated control mice, whereas mice treated with the Pam2-ODN combination
103 demonstrated profound antiviral protection (Figure 1A). Similarly, when isolated mouse lung epithelial
104 (MLE-15) cells were challenged with IAV 4 h after pretreatment with the individual ligands, we observed
105 no significant reductions in the viral burden relative to PBS treated cells. However, cells pretreated with
106 Pam2-ODN showed a substantial reduction in viral nucleoprotein (NP) gene expression as assessed by
107 qPCR relative to host 18s gene (Figure 1B). Comparing the effect of dual ligand treatment (E_{AB}) to the
108 expected response additivity of the individual ligand treatments ($E_A + E_B$) (Foucquier *et al*, 2015) reveals
109 supra-additive effects on both *in vivo* survival benefits and *in vitro* viral clearance (Figure 1C). To better
110 understand the molecular mechanisms driving such unanticipated synergy, we developed OBIF as a
111 phenotype-driven model (Hasin *et al*, 2017) to understand favorable drug-drug interactions mediating
112 synergistic responses and outcomes.
113
114 **Development of a systems synergy model from experimental Omics data**
115 To formally test whether the effect of dual factors (F_{AB}: Pam2-ODN) is greater than the expected linear
116 sum of its individual factors (F_A: Pam2; F_B: ODN), an initial 2-level 2-factor (2^2) factorial design is required
117 (Slinker, 1998; Foucquier *et al*, 2015) (Figure 1D). Our strategy adapts the traditional analysis of variance
118 (ANOVA) approach into a model that links the empirical analysis of synergy (Slinker, 1998; Foucquier *et*
119 *al*, 2015) with the high-throughput capacity and high-dimensionality of Omics datasets (Coral *et al*, 2017;
120 Bardini *et al*, 2017). As summarized in Figure 1E, OBIF integrates statistical and biological interactions
121 in Omics data matrices from single vs. dual factor exposures, leveraging Omics screening to promote
122 discovery of the molecular drivers of synergy, and facilitating the biological validation of synergy
123 regulators. The analytical pipeline is freely available as an R package at GitHub

124 (www.github.com/evanslab/OBIF). Naturally, the experimental validation components must be tailored to
125 the individual tools and characteristics of the biological responses being studied.
126
127 **Figure 1. Omics-Based Interaction Framework: phenotype-driven synergy modeling and**
128 **framework overview.**
129 (A) Mouse survival of influenza A challenge following the indicated pretreatments. Dashed line indicates
130 additive effect of single ligand treatments over PBS. n = 15 mice/condition. (B) Virus burden of isolated
131 mouse lung epithelial cells after influenza A challenge following the indicated pretreatments. RQ, relative
132 quantification of viral nucleoprotein (NP) expression to host 18s. n = 6 samples/condition. (C) Plot of
133 response additivity from antiviral responses in panels A (left) and B (right). Synergistic effects are
134 reflected by E_{AB} greater than the expected linear sum ($E_A + E_B$, dashed line) of individual ligand effects,
135 antagonistic effects are observed when $E_{AB} < E_A + E_B$. (D) Generic Omics workflow for phenotype-driven
136 synergy modeling using a 22 experimental design. (E) Overview of OBIF, including (i) Omics screening
137 of features in a data matrix, (ii) discovery of feature clusters of molecular drivers, and (iii) experimental
138 validation of biologically relevant synergy regulators. * $P < 0.05$ compared to either condition, *** $P <$
139 0.0005 compared to either condition.
140
141 **Differentially expressed molecules reveal synergy-specific pathways**
142 To investigate the mechanisms underlying Pam2-ODN synergy, we used OBIF to re-analyze previously
143 published (Cleaver *et al*, 2014) lung homogenate transcriptomic data from mice inhalationally treated with
144 single vs. dual ligands (GSE28994). After model fitting for feature expression (Figure EV1), this analysis
145 identifies 3456 features as differentially expressed molecules (DEMs) 2 h after treatment with Pam2,
146 2941 DEMs after ODN treatment, and 3138 DEMs after treatment with Pam2-ODN (Figure 2A). Despite
147 the fact that 52% (1617/3138) of DEMs were shared by Pam2-ODN and the individual ligands, enrichment
148 analysis using IPA software revealed an overrepresentation of 12 canonical cellular immune response

149 and cytokine signaling pathways that were activated by Pam2-ODN but not by either or both single
150 ligands (Figure 2B). Of these, NF-κB signaling was the most enriched signaling pathway by Pam2-ODN
151 treatment. Although unsupervised hierarchical clustering consistently segregated the treatment groups
152 (Figure 2C), this approach alone did not reveal distinctive gene clusters to explain the synergistic
153 response, likely due to the 52% redundancy of DEMs between groups.
154

155 **Expression profiles summarize biological interactions and disentangle effectors of synergistic**
156 **functions**

157 Rather than relying on potentially redundant DEM clusters, OBIF classifies dual factor-induced DEMs
158 into eight expression profiles (EPs) that characterize cooperative and competitive biological interactions
159 of individual factors (Table 1). EPs are defined by expression directionality (up- or down-regulation) of
160 individual features and are not biased by the DEM expression analysis. Cooperative EPs have accordant
161 expression directionality induced by F_A and F_B, while competitive EPs have opposite directionalities
162 induced by F_A and F_B. Among the cooperative EPs, concordant profiles result when F_{AB} directionality
163 corresponds with the single factor effects (EPs I and II), and discordant profiles occur when F_{AB}
164 directionality opposes the single factors (III and IV). Alternatively, among the competitive EPs, factor-
165 dominant profiles are defined by F_{AB} directionality correspondence with one factor (F_A dominant, V and
166 VI; F_B dominant, VII and VIII). Principal component analysis (Figure 2D) demonstrates that concordant
167 EPs (I and II) were the most abundant in our dataset, followed by Pam2-dominant profiles (V and VI).
168 This abundance of EPs I and II better emphasizes the cooperative effects of both factors than does
169 conventional DEM clustering alone. In particular, the contribution of ODN to the synergistic combination
170 might otherwise be overlooked by DEM analysis, as it induces enrichment of far fewer signaling pathways
171 (Figure 2B) and has a greater clustering distance from Pam2-ODN samples (Figure 2C).
172

Expression Pattern Response		Fold Change			Expression Profiles
In single factor exposures	In dual factor exposures	F_A	F_B	F_{AB}	
Cooperative	Concordant	↑	↑	↑	I
		↓	↓	↓	II
	Discordant	↓	↓	↑	III
		↑	↑	↓	IV
Competitive	Factor A-Dominant	↑	↓	↑	V
		↓	↑	↓	VI
	Factor B-Dominant	↓	↑	↑	VII
		↑	↓	↓	VIII

Table 1. Expression profiles depict biological interactions during dual factor exposure.

Notably, enrichment analysis reveals that molecular effectors clustered by EPs correspond with Pam2-ODN-induced functions (Figure 2E), suggesting a biological basis for the synergy. Specifically, we found that features in profiles I and V contributed to host survival functions, immune activity and microbicidal activity. Considered from an organizational perspective, induction of resistance to infection at the organismal level correlated with features in profile I, at the cellular level with profile II, and by leukocytes with profile V.

Figure 2. Differentially expressed molecules and expression profiles reveal synergy-mediating pathways and functions.

(A) Euler diagram of differentially expressed molecules following single or dual treatment in mouse lung homogenates. (B) Most overrepresented activated canonical pathways after IPA enrichment of DEMs. (C) Heatmap of expression values of DEMs in A with expression profiles shown per feature (rows). (D) Principal component analysis of Pam2-ODN DEMs identified by expression profiles. (E) Top activated

189 (orange) and inhibited (blue) diseases and functions after IPA enrichment of expression profiles. FC, fold
190 change.
191
192 **Factorial effects analysis integrates biological and statistical interactions in EPs**
193 Analysis of factorial effects in a data matrix from single vs. dual factor exposures can statistically
194 differentiate whether stochastic feature expression in a combination is correlated with the effect of an
195 individual factor (simple main effect, SME) or their influence on each other (interaction effect) (Li *et al*,
196 2013; Mihret *et al*, 2014; Zhang *et al*, 2017). Based on this principle, OBIF performs full factorial analysis
197 through paired comparisons of calculated β coefficients in each condition to determine statistical
198 relationships (Hassall *et al*, 2018) and discover significant main effects during expression analysis and
199 multi-factor effects (SMEs and interaction effect) from contrast (Mee, 2009) analysis (Figure 3A). Using
200 this approach, main effects determined significant DEMs per condition, while multi-factor effects
201 explained whether Pam2-ODN DEMs and EPs resulted from SMEs and/or an interaction of individual
202 ligands (Figure 3B). This analysis showed that most features in concordant profiles (I and II) are
203 influenced by at least one multi-factor effect, while all features in discordant profiles (III and IV) are
204 influenced by all multi-factor effects simultaneously. Not surprisingly, Pam2-dominant (V and VI) and
205 ODN-dominant (VII and VIII) expression mainly results from their respective SMEs. This analysis also
206 revealed that 67% (2116/3138) of Pam2-ODN DEMs are driven by the interaction effect of Pam2 and
207 ODN as interacting DEMs (iDEMs) (Figure 3C). Thus, OBIF reconciled the biological interactions from
208 EPs with the statistical interactions from multi-factor effects of Pam2-ODN.
209
210 **SMEs accurately reproduce the regulatory network of combined exposures**
211 Downstream analyses of SMEs have the capacity to discern the contributing roles of individual factors to
212 a combination treatment (Hassall *et al*, 2018). Hence, Pam2-ODN DEMs with significant SMEs were
213 used for network analysis of upstream regulators that are activated (orange) or inhibited (blue) and up-

214 regulated (red) or down-regulated (green) (Figure 3D). Similar to our previous findings with DEMs (Figure
215 2B), transcription factors from many pathways were involved, though NF-κB family members remained
216 central elements of this network. Demonstrating the cross-Omics function of OBIF, a parallel analysis of
217 reverse-phase protein array (RPPA) data from single- or dual-treated human lung epithelial cells
218 identified the top phospho-signaling DEMs (Figure EV2), and cross-validated STAT3, RelA and cJun as
219 transcriptional units involved in the Pam2-ODN signaling network (Figure 3E).
220

221 **iDEMs identify non-additive features and synergy regulators**

222 Non-additivity results from strong interaction effects between two factors in a combination and gives rise
223 to synergistic or antagonistic responses (Slinker et al, 1998; Geary et al, 2013). iDEMs integrate this
224 principle during feature selection based on significant interaction effects between factors, allowing
225 quantification of synergistic and antagonistic expression in a narrower set of differentially expressed
226 features. OBIF builds on previous definitions of the combination index (CI) (Foucquier *et al*, 2015;
227 Goldstein *et al*, 2017) to fit the values of feature expression:

228 $$CI = | (Log_2FC\ F_{AB}) / (Log_2FC\ F_A + Log_2FC\ F_B) |$$

229 where CI is the absolute ratio of the log2 fold change of Pam-ODN-induced DEMs (F_{AB}) and the additivity
230 threshold of Pam2 (F_A) and ODN (F_B), allowing identification of both antagonistic (CI < 1) or synergistic
231 (CI > 1) features (Figure 3F). A log2 transformation of the CI then yields an interaction score (IS) that
232 quantifies the effect size of non-additive expression relative to the additivity threshold, and can be applied
233 to both antagonistic (IS < 0) and synergistic (IS > 0) iDEMs (Figure 3G). This allows more focused
234 enrichment analysis, in this case supporting NF-κB/RelA and AP-1/cJun as key transcriptional upstream
235 regulators of Pam2-ODN's interaction effect and synergistic expression (Figure 3H).
236

237 **Figure 3. Full factorial analysis reveals regulatory networks and molecular drivers of synergy.**

238 (A) Scheme of full factorial analysis performed by OBIF from β coefficients. (B) Venn diagram of Pam2-
239 ODN DEMs correlated by expression profiles classes and multi-factor effects. (C) Feature count and
240 percentage of Pam2-ODN iDEMs and non-iDEMs in B. (D) Network analysis of activated (orange) or
241 inhibited (blue), and up-regulated (red) or down-regulated (green) upstream regulators of Pam2-ODN
242 after IPA enrichment of SME. (E) Cross-Omics validation of regulators in D. Differentially expressed
243 phospho-signaling molecules were identified with OBIF from a reverse-phase protein array in human lung
244 epithelial cells. (F) Non-additive feature expression assessed by combination index (CI). Representative
245 genes and their CI values are shown. (G) Interaction score (IS) of iDEMs, reflecting antagonistic (IS < 0)
246 and synergistic (IS > 0) features. (H) Top activated (orange) or inhibited (blue) transcriptional regulators
247 after IPA enrichment of iDEMs. DEMs, differentially expressed molecules. iDEMs, interacting DEMs.
248 SME, simple-main effects.
249

250 **Experimental validation of molecular regulators of Pam2-ODN synergy**

251 Prompted by the foregoing results, we tested whether RelA and cJun were biologically relevant synergy
252 regulators of Pam2-ODN-induced epithelial resistance. The DNA-binding activity of NF-κB and AP-1
253 subunits in isolated human bronchial epithelial cells (HBEC-3kt) after stimulation with Pam2-ODN
254 confirmed that RelA and cJun activation was strongly increased after 15 minutes of treatment without
255 significant contribution of other family members (Figure 4A, Figure EV3A). Indeed, RelA and cJun
256 exhibited surprisingly similar activation kinetics after Pam2-ODN treatment, further supporting
257 cooperation or coordination (Figure 4B). Investigating this co-activation of non-redundant transcriptional
258 families, single-cell nuclear translocation of canonical p50/RelA and cFos/cJun dimers in HBEC-3kt was
259 assessed by imaging flow cytometry. We found that all transcriptional subunits exhibited an increased
260 nuclear translocation (similarity score > 2) after 15 minutes of Pam2-ODN treatment relative to the PBS-
261 treated cells (Figure 4C). However, neither Pam2 nor ODN alone induced the same magnitude of nuclear

262 translocation, whether assessed by similarity scores (Rd value) or by the percentage of translocated cells
263 (Figure 4D) relative to PBS treated cells.
264
265 **Discovery of novel NF-κB and AP-1 cooperation required for antiviral protection**
266 To differentiate transcriptional cooperation from coincidental transcription factor activation after Pam2-
267 ODN treatment, we assessed the Pam2-ODN-induced nuclear co-translocation of NF-κB and AP-1
268 complexes in the presence or absence of NF-κB inhibitor IMD-0354 (IMD). As expected, pre-treatment
269 with IMD alone reduced the Rd Value and percentage of translocated cells for RelA and p50 without
270 significantly modifying the percentage of translocation for cJun and cFos. However, NF-κB inhibition with
271 IMD also unexpectedly reduced the Pam2-ODN-induced similarity score shifts and nuclear translocation
272 of AP-1 subunits, particularly of cFos (Figure 4E). This indicates that NF-κB inhibition impaired Pam2-
273 ODN-induced AP-1 nuclear translocation, confirming the cooperative regulation of these two non-
274 overlapping signaling pathways. Representative images shown in Figure 4F demonstrate that inhibition
275 with IMD reduced Pam2-ODN-induced heterodimerization and nuclear translocation of NF-κB and AP-1
276 complexes. Further, we confirmed that disruption of this transcriptional cooperation was sufficient to
277 impair the inducible viral burden reduction seen with Pam2-ODN (Figure 4G).
278
279 **Figure 4. Regulators identified with OBIF uncovered cooperation between RelA and cJun that is**
280 **required for synergistic antiviral protection.**
281 (A) Transcription factor activity of NF-κB and AP-1 subunits 15 min after treatment of human lung
282 epithelial cells with Pam2-ODN. n = 3-6 samples/condition. (B) RelA and cJun activity at indicated times
283 after Pam2-ODN treatment. n = 6 samples/condition. (C) Nuclear translocation scores of NF-κB and AP-
284 1 heterodimers after Pam2-ODN treatment. Shown as normalized frequency of similarity score per
285 condition. (D) NF-κB and AP-1 subunit nuclear translocation in C (increased, red; decreased, blue) per
286 condition. (E) NF-κB and AP-1 subunit nuclear translocation with or without NF-κB inhibition by IMD-

287 0345. (F) Representative imaging flow cytometry images of hetero-dimerization and nuclear translocation
288 of NF-κB and AP-1 in D and E. (G) Virus burden of mouse lung epithelial cells challenged with influenza
289 A with or without NF-κB inhibition. n = 4 samples/condition. *, $P < 0.05$; **, $P < 0.005$; ***, $P < 0.0005$
290 compared to baseline.
291

292 **Application of OBIF across multiple platforms and conditions**

293 To demonstrate its generalizability, we used OBIF to analyze synergistic regulators in datasets derived
294 from microarray, RNA-seq, RPPA and mass spectrometry-based metabolomics investigations of diverse
295 factor classes and biological systems that demonstrate synergistic biological outcomes (Cleaver *et al*,
296 2014; Caetano *et al*, 2018; Singh *et al*, 2019; Han *et al*, 2019). As a preliminary step before full factorial
297 analysis of individual features, OBIF performs an interaction analysis between the two factors of interest
298 using a two-way ANOVA model to represent the impact of factorial effects at the whole "-ome" level. This
299 statistical summary shows the effects of individual factors and interactions through interaction plots and
300 statistical significance calculations (Figure 5A). This provides adjusted R^2 and F-statistic p-values of the
301 two-way ANOVA that allow evaluation of improved model fitness (Figure EV4 A) and detection of
302 interaction terms (Figure EV4 B) within a dataset. After confirming adequate model fitness (i.e. adjusted
303 $R^2 > 0.5$, F-test < 0.05), full factorial analysis on scaled data from targeted or non-targeted platforms
304 identifies DEMs (Figure 5B) from individual features with an increased discriminatory power for interaction
305 effects (Figure EV4C). EPs then represent the biological interactions of dual factor DEMs regardless of
306 their factor classes (Figure 5C). Contrast analysis is then applied to more adequately retrieve and classify
307 iDEMs (Figure EV4D) and interaction scores are calculated in a uniform scale whether the original data
308 contained continuous or count-based expression values (Figure 5D). Finally, OBIF visually summarizes
309 the results of full factorial analysis in a Circos plot to easily identify molecular drivers of synergy from the
310 co-expressed features, DEMs, log_2FC, EPs, multi-factor effects and iDEMs with their interaction score
311 (Figure 5E).

312

313 **Figure 5. OBIF reveals molecular drivers of synergy across platforms, factor classes and**
314 **experimental systems.**

315 (A) Interaction analysis of factorial effects at the whole "-ome" level, demonstrating interaction plots,
316 coefficient significance and quality of model fitness per platform. (B) Euler diagram of DEMs identified in
317 A. (C) Principal component analysis of dual factor DEMs in B clustered by EPs. (D) Interaction scores of
318 iDEMs in C. (E) Visual summary of molecular drivers of synergy in B-D plotted including DEMs, EPs and
319 iDEMs. E_F, feature expression; F_A, factor A; F_B, factor B; F_{AB}, factor AB; FC, fold change; DEMs,
320 differentially expressed molecules; EPs, expression profiles; iDEMs, interacting DEMs.

321

322 **DISCUSSION**

323 Synergistic and antagonistic interactions are common in nature and frequently promote efficacy of
324 therapeutic interventions (Chen *et al*, 2015; Ronzitti *et al*, 2018; Wei *et al*, 2018; Zappasodi *et al*, 2018;
325 Han *et al*, 2019). While synergy quantification methods from dose-response data, combinatorial
326 screening of molecule libraries, and other predictive exploration models may suggest potentially
327 synergistic conditions or treatments, they do not provide substantive insights into the molecular
328 mechanisms underlying synergy (Chen *et al*, 2015). Thus, synergy-mediating pathways cannot be
329 strategically targeted in rational drug development.

330

331 Our interest in synergy arose from our observations of the strikingly synergistic interactions of one such
332 empirically derived combination, Pam2-ODN. While we could easily quantify the superiority of protection
333 conferred by the dual treatment, in the absence of a systems theory to interrogate synergistic
334 mechanisms (Chen *et al*, 2015; Wei *et al*, 2018), we were limited in our capacity to use available Omics
335 datasets to deduce the mechanisms mediating the synergy. This is important because, although this lack
336 of mechanistic understanding does not limit the utility of the current combination, it precludes

337 development of next generation interventions that more precisely (perhaps, more efficaciously) target the
338 synergy-driving pathways with fewer off-target (potentially toxic) effects. In contrast to models that predict
339 possible synergy, OBIF was developed with the explicit intent to investigate established synergistic
340 events. As such, it is inherently a phenotype-driven model that performs full factorial analysis on feature
341 expression data from single vs. dual factor exposures to identify molecular clusters that reveal synergy-
342 mediating pathways, functions and regulators.
343
344 Using Pam2-ODN datasets as demonstrative examples, OBIF identified unanticipated transcriptional
345 cooperation between non-redundant transcription factors, RelA and cJun, as a molecular mechanism of
346 inducible synergistic protection against IAV. Thus, by facilitating understanding of combined factor
347 exposures in terms of the individual components, a computational discovery facilitated experimental
348 validation of a discrete, novel mediator of a non-additive biological response. Perhaps as importantly, the
349 computational analyses were accomplished by integration of data from different Omics platforms,
350 different specimen types, and even different host species.
351
352 Unlike most 2^2 designs, OBIF dissects factorial effects of dual factor exposures through full factorial
353 analysis of feature expression data in a single unsupervised step. This allows simultaneous identification
354 of DEMs directly from main effects of single or dual factors, overcoming pairwise comparisons to control
355 and repetitive analysis of each condition. While this simultaneous identification of DEMs can be
356 performed also with a mixed-effect model, we showed how this approach is suboptimal to detect
357 interaction effects at the level of individual features and iDEM selection when compared with full factorial
358 analysis. Additionally, clustering by DEMs, EPs and iDEMs improves the specificity of enrichment
359 analysis to disentangle the signaling pathways, functions and regulators of this synergistic combination
360 and to capture their specific driving features. Further, quantification of multi-factor effects (SMEs and

361 interaction effects) reveals whether particular features, molecular clusters or functions enriched by
362 synergistic combinations are the result of individual factors or their crosstalk.
363
364 These statistical relationships have biological analogues that are integrated by OBIF in the EP definitions.
365 In fact, profiles I and II rescued the underrepresentation of ODN observed in distance-based clustering
366 and enrichment analysis. Further, iDEMs derived from features with significant interaction effects allow
367 focusing discovery on synergy regulators and the calculation of interaction scores allows quantification
368 of their non-additive expression. Thus, unlike most systems models of synergy, OBIF facilitates
369 integrative analyses of biological and statistical interactions that are easily discoverable and interpretable
370 through molecular clusters representing the complex dynamics of synergistic combinations.
371
372 OBIF is available as an open-source R package with a semi-automated pipeline to facilitate its broad
373 application to unscaled original data from various Omics platforms, factor classes and biological systems.
374 We have shown that OBIF can be fitted to perform full factorial analysis and that it adequately identifies
375 DEMs, EPs, iDEMs and their attendant values and scores to promote discovery of molecular drivers of
376 synergy in multiple, diverse datasets.
377
378 In summary, OBIF provides a phenotype-driven systems biology model that allows multiplatform
379 dissection of molecular drivers of synergy. And, we encourage the application of OBIF to provide holistic
380 understanding in research fields where greater-than-additive beneficial combinations remain
381 understudied.
382
383 **MATERIALS AND METHODS**
384 **Reagents and Tools**

Reagent/Resource	Reference or Source	Identifier or Catalog Number
Experimental Models		
C57BL/6J (M. musculus)	Jackson Lab	B6.129P2Gpr37tm1Dgen/J
Immortalized human bronchial epithelial (HBEC-3kt) cells	Dr. John Minna	Authenticated by the MD Anderson Characterized Cell Line Core Facility
Murine lung epithelial (MLE-15) cells	Dr. Jeffrey Whitsett	Authenticated by the MD Anderson Characterized Cell Line Core Facility
Antibodies		
NFκB p50 (E-10) Alexa Fluor® 647	Santa Cruz Biotechnology, Inc.	Cat # sc-8414 AF647
NFκB p65 (F-6) Alexa Fluor® 488	Santa Cruz Biotechnology, Inc.	Cat # sc-8008 AF488
c-Jun (G-4) Alexa Fluor® 594	Santa Cruz Biotechnology, Inc.	Cat # sc-74543 AF594
c-Fos Antibody (D-1) Alexa Fluor® 546	Santa Cruz Biotechnology, Inc.	Cat # sc-8047 AF546
Oligonucleotides and sequence-based reagents		
Mouse 18s - Forward Primer	Sigma-Aldrich	5'-CTCATCCTTTATGACAAAGAAG-3'
Mouse 18s - Reverse Primer	Sigma-Aldrich	5'-AGATCATCATGTGAGTCAGAC-3'
Influenza NP - Forward Primer	Sigma-Aldrich	5'-GTAACCCGTTGAACCCCATT-3'
Influenza NP - Reverse Primer	Sigma-Aldrich	5'-CCATCCAATCGGTAGTAGCG-3'
Chemicals, enzymes and other reagents		
eBioscience™ Foxp3 / Transcription Factor Staining Buffer Set	Thermo Fisher Scientific	Cat # 00-5523-00

LIVE/DEAD™ Fixable Near-IR Dead Cell Stain Kit	Thermo Fisher Scientific	Cat # L34975
Power SYBR Green PCR Master Mix	Thermo Fisher Scientific	Cat # 4368702
UltraComp eBeads™ Compensation Beads	Thermo Fisher Scientific	Cat # 01-2222-42
RNAlater	Sigma-Aldrich	Cat # R0901-500ML
Accutase solution	Sigma-Aldrich	Cat # A6964-500ML
IMD-0354	Sigma-Aldrich	Cat # I3159-5MG
iScript™ cDNA Synthesis Kit	Bio-Rad	Cat # 1708891BUN
Software		
Rstudio	RStudio, Inc.	Version 1.2.5033
R	www.R-project.org	Version 3.6.3
Ingenuity Pathway Analysis	QIAGEN	Version 51963813
Prism 8	GraphPad Software, LLC.	Version 8.4.2
Amnis® IDEAS®	Luminex Corporation	Version 6.1
INSPIRE ImageStreamX	Luminex Corporation	System Software
KCJunior	Bio-Tek Instruments, Inc.	System Software
CFX Maestro™ Software	Bio-Rad	Cat # #12004110
Kits, instrumentation, laboratory equipment and other		
TransAM NFκB Family	Active Motif	Cat # 43296
TransAM AP-1 Family	Active Motif	Cat # 44296

TransAM STAT Family	Active Motif	Cat # 42296
RNeasy Mini Kit	Qiagen	Cat # 74106
QIAshredder	Qiagen	Cat # 79656
CFX Connect Real-Time PCR Detection System	Bio-Rad	Cat # 1855201
uQuant Universal Microplate Spectrophotometer	Bio-Tek Instruments, Inc.	Cat # MQX200
TProfessional TRIO combi PCR Thermocycler	Biometra	Cat # 070-724
NanoDrop™ One Microvolume UV-Vis Spectrophotometer	Thermo Fisher Scientific	Cat # ND-ONE-W
Amnis® ImageStream®XMk II	Luminex Corporation	Serial # ISX325

385 **Table 2. List of Reagents and Tools**

386

387 **Experimental Models**

388 *Animals*

389 All mouse experiments were performed with 6-10 week old C57BL/6J mice of a single sex in accordance
390 with the Institutional Animal Care and Use of Committee of The University of Texas MD Anderson Cancer
391 Center, protocol 00000907-RN01.

392

393 *Cell culture*

394 Immortalized human bronchial epithelial (HBEC-3kt) cells were kindly provided by Dr. John Minna.
395 HBEC-3kt cells were cultured in keratinocyte serum-free media (KSFM) supplemented with human
396 epidermal growth factor and bovine pituitary extract. Murine lung epithelial (MLE-15) cells were kindly

397 provided by Dr. Jeffrey Whitsett. The cell lines used were authenticated by the MD Anderson
398 Characterized Cell Line Core Facility. MLE-15 cells were cultured in RPMI supplemented with 10% fetal
399 bovine serum. Cultures were maintained in the presence of penicillin and streptomycin.
400
401 **Exposure to TLR ligands**
402 S-[2,3-bis(palmitoyloxy)-propyl]-(R)-cysteinyl-(lysyl) 3-lysine (Pam2 CSK4) and ODN M362 were
403 reconstituted in endotoxin-free water, then diluted to the desired concentration in sterile PBS. For in vivo
404 experiments, as previously described (Kirkpatrick et al, 2018; Ware et al, 2019), the indicated ligands
405 were placed in an Aerotech II nebulizer driven by 10L/min air supplemented with 5% CO2 for 20 min.
406 The nebulizer was connected by polyethylene tubing to a polyethylene exposure chamber. 24 h prior to
407 infections, 10 ml of Pam2 (4 μM) and/or ODN (1 μM) was delivered via nebulization to unrestrained mice
408 for 20 minutes, and then mice were returned to normal housing. For in vitro experiments, Pam2-ODN
409 was added to the culture media 4 h prior to inoculation with virus.
410
411 **Reverse-Phase Protein Array**
412 To simultaneously evaluate the expression of 161 regulatory proteins and phospho-proteins in HBEC-3kt
413 cells after exposure to either PBS, Pam2, ODN or Pam2-ODN, a targeted high-throughput screening
414 proteomic assay was performed by the Reverse Phase Protein Array Core Facility at The University of
415 Texas MD Anderson Cancer Center (Tibes *et al*, 2006; Hennessy *et al*, 2010). The RPPA included 4
416 biological replicates per treatment condition, and data is available at GitHub
417 (www.github.com/evanslab/OBIF).
418
419 **Infection Models**
420 For in vivo infections, frozen stock (2.8 × 107 50% tissue culture infective doses [TCID50] ml−1) of
421 influenza A H3N2, virus was diluted 1:250 in 0.05% gelatin in Eagle's minimal essential medium and

422 delivered by aerosolization for 20 min to achieve a 90% lethal dose (LD90) to LD100 (~100 TCID50 per
423 mouse). Mouse health was followed for 21 d post infection. n = 15 mice per condition. Animals were
424 weighed daily and sacrificed if they met euthanasia criteria, including signs of distress or loss of 20% pre-
425 infection body weight. For in vitro infections, IAV (multiplicity of infection [MOI] of 1.0) was added to cells
426 in submerged monolayer and viral burden was assessed 24 hours post infection.
427
428 **Pathogen burden quantification**
429 To measure transcript levels of IAV nucleoprotein (NP) gene, samples were harvested in RNAlater and
430 RNA was extracted using the RNeasy extraction kit. 500 ng total RNA was reverse transcribed to cDNA
431 by using an iScript cDNA synthesis kit and submitted to quantitative reverse transcription-PCR (RT-PCR)
432 analysis with SYBR green PCR master mix on an ABI ViiA 7 real-time PCR system. Host 18S rRNA was
433 similarly probed to determine relative expression of viral transcripts.
434
435 **Omics Dataset Formatting**
436 OBIF's input in R requires an analysis-ready data matrix m with expression values and of dimensions f x
437 n, where f is the number of features as rows and n is the number of samples S as columns. The
438 appropriate sample order in dimensions n of m is:
439 $$n = S_{(0,0)}^{1} + \ldots + S_{(0,0)}^{i} + S_{(1,0)}^{1} + \ldots + S_{(1,0)}^{i} + S_{(0,1)}^{1} + \ldots + S_{(0,1)}^{i} + S_{(1,1)}^{1} + \ldots + S_{(1,1)}^{i}$$
440 The subscripts denote the condition of the samples: exposed to neither factor (0,0), exposed to factor A
441 alone (1,0), exposed to factor B alone (0,1) or exposed to both factors A and B (1,1). The superscripts
442 represent the sample replicates from 1 to i within each of the four conditions.
443
444 To improve detection of interaction effects, OBIF allows sequential transformation of an unscaled original
445 data matrix with background correction, log2-transformation, quantile normalization or a combination of
446 these if needed. Background correction reduces noise to signal ratio at the lower limits of detection and

447 methods vary per platform with code extensions are available at GitHub for microarray data using the
448 lumi package, and for count-based sequencing data using rpm, rpkm, fpkm and tpm thresholds. Log2-
449 transformation of continuous and count-base data is incorporated to provide a Gaussian-like data
450 distribution, and quantile normalization is used to minimize the variance between samples during data
451 scaling (Lo *et al*, 2015; Abrams *et al*, 2019) with OBIF to meet the statistical assumptions needed for two-
452 way ANOVA analysis of interaction terms in a dataset (Slinker, 1998; Foucquier *et al*, 2015).
453
454 **Interaction analysis**
455 To evaluate significant interaction terms between factors at the whole "-ome" level, OBIF performs a
456 multiple linear regression across the expression values in a dataset:
457 $$E_O \sim 0 + F_A + F_B + F_A \cdot F_B$$
458 where the interaction analysis of the Omics expression levels (E_O) is equivalent to a two-way ANOVA
459 analysis where the intercept is referenced to the control samples (0) and returns a statistical summary of
460 terms for the individual factor A (F_A), factor B (F_B) and their interaction ($F_A \cdot F_B$). Goodness of fit is
461 calculated from the adjusted R^2 values, and overall significance is determined by the p-values of F-
462 statistics of the regression. Unscaled original data and scaled data with OBIF are compared to evaluate
463 improvement in detection of significant interaction terms in a given dataset.
464
465 **Full Factorial Analysis**
466 *Expression Analysis*
467 To perform differential expression analysis for detection of DEMs, OBIF fits a fixed-effects model to the
468 expression data of each feature:
469 $$E_f = \beta_0 + \beta_1 \cdot F_A + \beta_2 \cdot F_B + \beta_3 \cdot F_{AB}$$
470 where the expression level of features (E_f) is a function of the estimated β coefficients for the main effects
471 of individual factor A (F_A) and factor B (F_B) and their combination (F_{AB}). After regression, empirical

472 Bayesian shrinkage of the standard errors is used to stabilize inferences of t-statistics, F-statistics, and
473 log-odds used for differential expression analysis. Q-values are then calculated using the Benjamini and
474 Hochberg method to reduce the false discovery rate (FDR). Alternatively, code extensions for are
475 available at GitHub to perform Bonferroni corrections or calculate Tukey Honest Significant Differences
476 adjustment for multiple testing instead of FDR.

477

478 *Contrast analysis*

479 To analyze the remaining factorial effects in the fitted linear model of feature expression, the coefficients
480 and standard errors will be estimated typical of a two-way ANOVA from a set of contrasts that define the
481 SMEs of each factor and their interaction effect:

482 $$SME\ of\ F_A = \beta_3 \cdot F_{AB} - \beta_2 \cdot F_B$$

483 $$SME\ of\ F_B = \beta_3 \cdot F_{AB} - \beta_1 \cdot F_A$$

484 $$Interaction\ effect\ of\ F_A \cdot F_B\ (\beta_4) = \beta_3 \cdot F_{AB} - \beta_2 \cdot F_B - \beta_1 \cdot F_A$$

485 The standard errors calculated use a significance threshold (p-value < 0.05) to determine if DEMs with
486 F_{AB} (Pam2-ODN) are susceptible to SME or interaction effects. Selection of iDEMs is based on DEMs of
487 F_{AB} with a significant interaction effect.

488

489 **Mixed-effects model**

490 To evaluate performance of full factorial analysis with OBIF, detection of interaction effects at the level of
491 individual features is compared to a mixed-effect model (Caetano *et al*, 2018):

492 $$E_{f\text{-}Mix} = \beta_0 + \beta_1 \cdot F_A + \beta_2 \cdot F_B + \beta_4 \cdot F_A \cdot F_B + (1|S)$$

493 where the expression level of features in a mixed-effect model ($E_{f\text{-}Mix}$) is a function of the estimated β
494 coefficients for the fixed effects of individual factor A (F_A) and factor B (F_B) and their interaction ($F_A \cdot F_B$)
495 with a random effect (1|S) for all sample conditions ($S_{(0,0)}$, $S_{(1,0)}$, $S_{(0,1)}$, $S_{(1,1)}$). After regression, empirical
496 Bayesian shrinkage of the standard errors is used to stabilize inferences of t-statistics and F-statistics.

497 The standard errors calculated from the interaction term use a significance threshold (p-value < 0.05) to
498 determine significant interaction effects.
499
500 **Beta-uniform mixture model**
501 Interaction p-values are extracted from the interaction term of mixed-effects model and from the
502 interaction effect contrast of full factorial analysis. Independently, a beta-uniform mixture model is fitted
503 to these sets of p-values (Pounds *et al*, 2003; Ji *et al*, 2005) to compare their discrimination ability using
504 their receiver operating characteristic area under the curve (ROC AUC). Using the beta-uniform mixture
505 models, we calculated the number of true positives (TP), false positive (FP) and false negatives (FN)
506 detections (Pounds *et al*, 2003; Zhang *et al*, 2012) at the threshold level of iDEM selection (interaction p-
507 value = 0.05) to estimate their precision and recall proportion:
508 $$Precision = TP / (TP + FP)$$
509 $$Recall = TP / (TP + FN)$$
510
511 **Unsupervised clustering of features with OBIF**
512 *Hierarchical clustering and heatmaps of DEMs*
513 All DEMs were represented in heatmaps after hierarchically clustering using Ward's minimum variance
514 method with Euclidean distances of $\log_2$FC values to compute dissimilarity by rows (features) and by
515 columns (samples). Column dendrograms were plotted to represent the distance between samples,
516 vertical side bar colors summarize DEMs according to their and horizontal side bars colors represent
517 sample types by factors. Color scale keys indicate the levels of feature expression with upregulation in
518 red and downregulation in green.
519
520 *Principal component analysis of expression profiles*

521 DEMs with F_{AB} (Pam2-ODN) were clustered by principal component analysis based on the mean linear
522 fold change difference to reveal the expression patterns biologically present across all factors FA, FB
523 and FAB. Principal components 1 and 2 were used for plotting DEMs with FAB and the variability between
524 features is marked in each axis. EPs were identified in the clusters for each individual feature according
525 to Table 1.
526
527 **Enrichment analysis**
528 To provide biological interpretation of the full factorial analysis and classification of features, enrichment
529 analysis was integrated in the pipeline to determine candidate effectors and regulators of synergy,
530 biological pathways and functional processes. Sets for DEMs, EPs, DEMs with SMEs and iDEMs are
531 uploaded independently, and enrichment analysis is performed with IPA software (QIAGEN, Hilden,
532 Germany) for core analysis using the expression levels of features. Both gene and chemical Ingenuity
533 Knowledge Base modules are used as enrichment reference, considering only experimentally observed
534 confidence levels for identification of direct and indirect relationships. The thresholds of significance for
535 canonical pathways, upstream analysis, diseases & functions, regulator effects and network analysis are
536 ≥ 2 for activation z-score and < 5% false discovery rates for all predictions.
537
538 **DNA-binding ELISA**
539 HBEC-3kt were grown to 80-100% confluence in 24-well plates and treated with PBS, Pam2, ODN, or
540 Pam2-ODN for the indicated durations. Measurements of DNA-binding of members of NF-κB and AP-1
541 transcription factor members from whole cell lysates were made using their respective TransAM Kit
542 according to product directions. For signal detection, samples were read immediately for absorbance at
543 450 nm with reference wavelength at 655 nm on a microplate reader. Experiments were repeated in
544 triplicate and statistical analysis was performed with unpaired student's t test using GraphPad Prism 8.0
545 with a significance threshold of p-value <0.05.

546

547 **Detection of Nuclear Translocation**

548 *Transcription factor staining and image acquisition*

549 HBEC-3kt were grown to 80-100% confluence in 100mm dishes and treated for 30 min with PBS, Pam2,
550 ODN or Pam2-ODN with or without pretreatment with NF-κB inhibitor IMD-0354 at 25 ng/µL for 16 h.
551 Cells were detached from the plate with a 5 min incubation at 37 ºC degrees with 3 ml of Accutase to
552 prevent additional activation of transcriptional activity. Cells were pelleted in individual 15 ml tubes at 500
553 g for 5 min and suspended in 500 µL of eBioscience FOXP3 fixation/permeabilization buffer for 15 min
554 at room temperature. Cells were stained with a LIVE/DEAD Fixable Near IR Dead Cell Dye and with a
555 1:1000 dilution of NF-κB p50 (E-10) Alexa Fluor 647, NF-κB p65 (F-6) Alexa Fluor 488, c-Jun (G-4) Alexa
556 Fluor 594 and c-Fos (D-1) Alexa Fluor 546 conjugated antibodies for 1 h on ice and protected from light.
557 After incubation, cells were pelleted and washed with 200 µL of sterile PBS 4 times, then resuspended
558 in 100 µL sterile PBS. After the last wash, cells were pelleted and resuspended in 50 µL of sterile PBS
559 and nuclear DAPI staining at 0.5 µg/mL was performed just prior to data acquisition on ImageStreamX
560 MII.

561

562 *Data acquisition with ImageStreamX MKII*

563 HBEC-3kt images were acquired using INSPIRE software on the ImagestreamX Mark II imaging flow
564 cytometer (Amnis Corporation) at 40× magnification, with lasers 405 nm (85.00 mW), 488 nm
565 (200.00 mW), and side scatter (782 nm) (1.14 mW). 10,000 images per sample acquired include a
566 brightfield image (Channel 1 and 9), p65 Alexa Fluor 488 (Channel 2), c-Fos Alexa Fluor 546 (Channel
567 3), c-Fos Alexa Fluor 594 (Channel 4), side scatter (Channel 6), DAPI (Channel 7), and p50 Alexa Fluor
568 647 (Channel 3). The laser outputs prevented saturation of pixels in the relevant detection channels as
569 monitored by the corresponding Raw Max Pixel features during acquisition. For image compensation,
570 single color controls were stained with all fluorochromes and 500 events were recorded with each laser

571 for individual controls. Fluorescent images were taken in all channels with brightfield LEDs and scatter
572 lasers turned off to accurately capture fluorescence. Individual single-color control file was then merged
573 to generate a compensation matrix and all sample files were processed with this matrix applied.
574
575 *Nuclear translocation analysis*
576 After compensation for spectral overlap based on single color controls, analysis was performed and
577 individual cell images were created using IDEAS® software version 6.1. Cell populations were
578 hierarchically gated first by single cells, then cells in focus, then negative selected for live cells, and finally
579 as double positive for both DAPI and the transcription factor subunit of interest (Figure EV3B). The spatial
580 relationship between the transcription factors and nuclear images was measured using the 'Similarity'
581 feature in the IDEAS software to quantitate the mean similarity score in the cell populations per sample.
582 A similarity score >1 represents nuclear translocation, and the shift in distribution of nuclear translocation
583 between two samples was calculated using the Fisher's Discriminant ratio (Rd value) (Maguire *et al*,
584 2015).
585
586 **ACKNOWLEDGEMENTS**
587 The research reported here was supported by The University of Texas System and Mexico's Consejo
588 Nacional de Ciencia Y Tecnología (CONACYT) through the ConTex Postdoctoral Fellowship Program to
589 J.P.G., by NIH grants R01 HL117976, DP2 HL123229 and R35 HL144805 to S.E.E. and by
590 P30CA016672 to MD Anderson Cancer Center. The opinions expressed are those of the authors and do
591 not represent views of these funding agencies. The Functional Proteomics RPPA Core facility is
592 supported by MD Anderson Cancer Center Support Grant # 5 P30 CA016672-40. The Advanced
593 Cytometry & Sorting Core Facility is supported by NCI P30CA016672 and is equipped for Imaging Flow
594 Cytometry at MD Anderson Cancer Center. J.P.G. acknowledges and thanks the Methods in
595 Epidemiologic, Clinical and Operations Research (MECOR) Program from the American Thoracic Society

596 (ATS) and Asociación Latinoamericana de Tórax (ALAT) for their support and dedication in building
597 research capacity in Latin America and other countries around the globe, particularly to their faculty Dr.
598 Fernando Holguin and Dr. Altay Souza for their critical feedback.

599

600 **AUTHOR CONTRIBUTIONS**

601 Conforming to the ICMJE criteria, all authors gave approval of the final version to be published and
602 contributed to writing or revising the article critically for important intellectual content. J.P.G. and S.E.E.
603 conceived the project and wrote the manuscript; J.P.G. conceived, implemented and validated the model;
604 J.P.G., V.V.K., T.C.R. and S.J.W. performed in vitro and in vivo experiments; J.P.G., V.V.K., T.C.R.,
605 S.W., S.J.W., J.Z., J.W., Y.W. and S.E.E. interpreted results; S.W., R.S., M.S.C., S.J.M., and F.M.J.
606 generated datasets for analysis and validation of the model; J.PG., J.Z. and J.W. performed
607 bioinformatics analyses; Y.W. and S.E.E. supervised the project.

608

609 **CONFLICTS OF INTEREST**

610 S.E.E. is an author on U.S. patent 8,883,174 “Stimulation of Innate Resistance of the Lungs to Infection
611 with Synthetic Ligands” and owns stock in Pulmotect Inc., which holds the commercial options on these
612 patent disclosures. All other authors declare that no conflict of interest exists.

613

614 **REFERENCES**

615 Abrams, Z. B., Johnson, T. S., Huang, K., Payne, P. R. O., & Coombes, K. (2019). A protocol to evaluate
616 RNA sequencing normalization methods. BMC Bioinformatics, 20(Suppl 24), 679. doi:10.1186/s12859-
617 019-3247-x

618 Antony, J. (2014). 6 - Full Factorial Designs. In J. Antony (Ed.), Design of Experiments for Engineers and
619 Scientists (Second Edition) (pp. 63-85). Oxford: Elsevier.

620 Bardini, R., Politano, G., Benso, A., & Di Carlo, S. (2017). Multi-level and hybrid modelling approaches
621 for systems biology. Computational and Structural Biotechnology Journal, 15, 396-402.
622 doi:https://doi.org/10.1016/j.csbj.2017.07.005
623 Caetano, M. S., Hassane, M., Van, H. T., Bugarin, E., Cumpian, A. M., McDowell, C. L., Cavazos, C. G.,
624 Zhang, H., Deng, S., Diao, L., Wang, J., Evans, S. E., Behrens, C., Wistuba, I. I., Fuqua, S., Lin, H.,
625 Stabile, L. P., Watowich, S. S., Kadara, H., & Moghaddam, S. J. (2018). Sex specific function of
626 epithelial STAT3 signaling in pathogenesis of K-ras mutant lung cancer. Nature communications, 9(1),
627 4589. https://doi.org/10.1038/s41467-018-07042-y
628 Chen, D., Liu, X., Yang, Y., Yang, H., & Lu, P. (2015). Systematic synergy modeling: understanding drug
629 synergy from a systems biology perspective. BMC Syst Biol, 9, 56. doi:10.1186/s12918-015-0202-y
630 Cleaver, J. O., You, D., Michaud, D. R., Pruneda, F. A., Juarez, M. M., Zhang, J., . . . Evans, S. E. (2014).
631 Lung epithelial cells are essential effectors of inducible resistance to pneumonia. Mucosal Immunol,
632 7(1), 78-88. doi:10.1038/mi.2013.26
633 Collaborators, G. L. (2017). Estimates of the global, regional, and national morbidity, mortality, and
634 aetiologies of lower respiratory tract infections in 195 countries: a systematic analysis for the Global
635 Burden of Disease Study 2015. The Lancet. Infectious diseases, 17(11), 1133-1161.
636 doi:10.1016/S1473-3099(17)30396-1
637 Coral, C., & Bokelmann, W. (2017). The Role of Analytical Frameworks for Systemic Research Design,
638 Explained in the Analysis of Drivers and Dynamics of Historic Land-Use Changes. Systems, 5(1).
639 doi:10.3390/systems5010020
640 Das, A. K., & Dewanjee, S. (2018). Chapter 3 - Optimization of Extraction Using Mathematical Models
641 and Computation. In S. D. Sarker & L. Nahar (Eds.), Computational Phytochemistry (pp. 75-106):
642 Elsevier.

643 Duggan, J. M., You, D., Cleaver, J. O., Larson, D. T., Garza, R. J., Guzman Pruneda, F. A., . . . Evans,
644 S. E. (2011). Synergistic interactions of TLR2/6 and TLR9 induce a high level of resistance to lung
645 infection in mice. J Immunol, 186(10), 5916-5926. doi:10.4049/jimmunol.1002122
646 Foucquier, J., & Guedj, M. (2015). Analysis of drug combinations: current methodological landscape.
647 Pharmacol Res Perspect, 3(3), e00149. doi:10.1002/prp2.149
648 Geary, N. (2012). Understanding synergy. American Journal of Physiology-Endocrinology and
649 Metabolism, 304(3), E237-E253. doi:10.1152/ajpendo.00308.2012
650 Goldstein, I., Paakinaho, V., Baek, S., Sung, M.-H., & Hager, G. L. (2017). Synergistic gene expression
651 during the acute phase response is characterized by transcription factor assisted loading. Nature
652 Communications, 8(1), 1849. doi:10.1038/s41467-017-02055-5
653 Han, M.-L., Liu, X., Velkov, T., Lin, Y.-W., Zhu, Y., Creek, D. J., . . . Li, J. (2019). Comparative
654 Metabolomics Reveals Key Pathways Associated With the Synergistic Killing of Colistin and Sulbactam
655 Combination Against Multidrug-Resistant Acinetobacter baumannii. Frontiers in Pharmacology,
656 10(754). doi:10.3389/fphar.2019.00754
657 Hasin, Y., Seldin, M., & Lusis, A. (2017). Multi-omics approaches to disease. Genome Biol, 18(1), 83.
658 doi:10.1186/s13059-017-1215-1
659 Hassall, K. L., & Mead, A. (2018). Beyond the one-way ANOVA for 'omics data. BMC Bioinformatics,
660 19(Suppl 7), 199. doi:10.1186/s12859-018-2173-7
661 Hennessy, B. T., Lu, Y., Gonzalez-Angulo, A. M., Carey, M. S., Myhre, S., Ju, Z., Davies, M. A., Liu, W.,
662 Coombes, K., Meric-Bernstam, F., Bedrosian, I., McGahren, M., Agarwal, R., Zhang, F., Overgaard, J.,
663 Alsner, J., Neve, R. M., Kuo, W. L., Gray, J. W., Borresen-Dale, A. L., … Mills, G. B. (2010). A Technical
664 Assessment of the Utility of Reverse Phase Protein Arrays for the Study of the Functional Proteome in
665 Non-microdissected Human Breast Cancers. Clinical proteomics, 6(4), 129–151.
666 https://doi.org/10.1007/s12014-010-9055-y

667 Kirkpatrick, C. T., Wang, Y., Leiva Juarez, M. M., Shivshankar, P., Pantaleon Garcia, J., Plumer, A. K., .
668 . . Evans, S. E. (2018). Inducible Lung Epithelial Resistance Requires Multisource Reactive Oxygen
669 Species Generation To Protect against Viral Infections. MBio, 9(3). doi:10.1128/mBio.00696-18
670 Li, C., Shen, W., Shen, S., & Ai, Z. (2013). Gene expression patterns combined with bioinformatics
671 analysis identify genes associated with cholangiocarcinoma. Comput Biol Chem, 47, 192-197.
672 doi:10.1016/j.compbiolchem.2013.08.010
673 Li, O. T. W., Chan, M. C. W., Leung, C. S. W., Chan, R. W. Y., Guan, Y., Nicholls, J. M., & Poon, L. L. M.
674 (2009). Full factorial analysis of mammalian and avian influenza polymerase subunits suggests a role
675 of an efficient polymerase for virus adaptation. PLOS ONE, 4(5), e5658-e5658.
676 doi:10.1371/journal.pone.0005658
677 Lo, S., & Andrews, S. (2015). To transform or not to transform: using generalized linear mixed models to
678 analyse reaction time data. Front Psychol, 6, 1171. doi:10.3389/fpsyg.2015.01171
679 Maguire, O., O'Loughlin, K., & Minderman, H. (2015). Simultaneous assessment of NF-κB/p65
680 phosphorylation and nuclear localization using imaging flow cytometry. Journal of immunological
681 methods, 423, 3-11. doi:10.1016/j.jim.2015.03.018
682 Mee, R. W. (2009). Analysis of Full Factorial Experiments. In R. Mee (Ed.), A Comprehensive Guide to
683 Factorial Two-Level Experimentation (pp. 27-74). New York, NY: Springer New York.
684 Metlay, J. P., Waterer, G. W., Long, A. C., Anzueto, A., Brozek, J., Crothers, K., . . . Whitney, C. G.
685 (2019). Diagnosis and Treatment of Adults with Community-acquired Pneumonia. An Official Clinical
686 Practice Guideline of the American Thoracic Society and Infectious Diseases Society of America.
687 American journal of respiratory and critical care medicine, 200(7), e45-e67. doi:10.1164/rccm.201908-
688 1581ST
689 Mihret, A., Loxton, A. G., Bekele, Y., Kaufmann, S. H. E., Kidd, M., Haks, M. C., . . . Walzl, G. (2014).
690 Combination of gene expression patterns in whole blood discriminate between tuberculosis infection
691 states. BMC Infectious Diseases, 14(1), 257. doi:10.1186/1471-2334-14-257

692 Ronzitti, G., & Mingozzi, F. (2018). Combination Therapy Is the New Gene Therapy? Molecular therapy
693 : the journal of the American Society of Gene Therapy, 26(1), 12-14. doi:10.1016/j.ymthe.2017.12.008
694 Singh, R., Peng, S., Viswanath, P., Sambandam, V., Shen, L., Rao, X., . . . Johnson, F. M. (2019). Non-
695 canonical cMet regulation by vimentin mediates Plk1 inhibitor–induced apoptosis. EMBO Molecular
696 Medicine, 11(5), e9960. doi:10.15252/emmm.201809960
697 Slinker, B. K. (1998). The statistics of synergism. Journal of molecular and cellular cardiology, 30(4), 723-
698 731. doi:10.1006/jmcc.1998.0655
699 Tibes, R., Qiu, Y., Lu, Y., Hennessy, B., Andreeff, M., Mills, G. B., & Kornblau, S. M. (2006). Reverse
700 phase protein array: validation of a novel proteomic technology and utility for analysis of primary
701 leukemia specimens and hematopoietic stem cells. Molecular cancer therapeutics, 5(10), 2512–2521.
702 https://doi.org/10.1158/1535-7163.MCT-06-0334
703 Tuvim, M. J., Gilbert, B. E., Dickey, B. F., & Evans, S. E. (2012). Synergistic TLR2/6 and TLR9 activation
704 protects mice against lethal influenza pneumonia. PLOS ONE, 7(1), e30596-e30596.
705 doi:10.1371/journal.pone.0030596
706 Ware, H. H., Kulkarni, V. V., Wang, Y., Pantaleón García, J., Leiva Juarez, M., Kirkpatrick, C. T., . . .
707 Evans, S. E. (2019). Inducible lung epithelial resistance requires multisource reactive oxygen species
708 generation to protect against bacterial infections. PLOS ONE, 14(2), e0208216.
709 doi:10.1371/journal.pone.0208216
710 Wei, P. L., Gu, H., Liu, J., & Wang, Z. (2018). Development of Fangjiomics for Systems Elucidation of
711 Synergistic Mechanism Underlying Combination Therapy. Comput Struct Biotechnol J, 16, 565-572.
712 doi:10.1016/j.csbj.2018.10.015
713 Zappasodi, R., Merghoub, T., & Wolchok, J. D. (2018). Emerging Concepts for Immune Checkpoint
714 Blockade-Based Combination Therapies. Cancer Cell, 34(4), 690. doi:10.1016/j.ccell.2018.09.008

715 Zhang, J., & Coombes, K. R. (2012). Sources of variation in false discovery rate estimation include
716 sample size, correlation, and inherent differences between groups. BMC Bioinformatics, 13 Suppl 13,
717 S1. doi:10.1186/1471-2105-13-S13-S1
718 Zhang, X., Cha, I.-H., & Kim, K.-Y. (2017). Use of a Combined Gene Expression Profile in Implementing
719 a Drug Sensitivity Predictive Model for Breast Cancer. Cancer Res Treat, 49(1), 116-128.
720 doi:10.4143/crt.2016.085

721 **SUPPORTING EXTENDED VERSION FIGURE LEGENDS**

722 **Figure EV1. Overview of model fitting of Omics datasets during analysis with OBIF.**

723 (A) Quality control plots assess data distribution of GSE28994 with violin plots (*top*) and detect potential
724 outliers by hierarchical clustering (*bottom*) in both the pre-processed original dataset (*left*) and the
725 analysis-ready dataset (*right*). (B) Interaction analysis of factorial effects at the whole transcriptome level,
726 demonstrating interaction plots, coefficient significance and goodness of fit per platform. (C)
727 Representative volcano plots of full factorial analysis from analysis ready data for each condition after
728 expression analysis (*top*) and Q-Q plots of moderated t-statistics for each multi-factor effect after contrast
729 analysis (*bottom*). (D) Visual summary of OBIF's outputs including DEMs, EPs and iDEMs (*left*) plotted
730 into 3 rings (*right*): (i) DEMs, where inner links represent shared features between DEMs followed by their
731 log_2FC values; (ii) EPs, where inner sectors represent individual profiles (I to VIII) followed by their of
732 significant F_A-SME (green), F_B-SME (orange) or $F_A \cdot F_B$ interaction effect (pink); and (iii) iDEMs,
733 represented by their synergistic or antagonistic interaction scores. FC, fold change; DEMs, differentially
734 expressed molecules; EPs, expression profiles; iDEMs, interacting DEMs; SME, simple main effect.

735

736 **Figure EV2. OBIF analysis of RPPA data from HBEC-3kt treated with single or dual ligands.**

737 (A) Interaction analysis of factorial effects at the whole proteome level, demonstrating interaction plots,
738 coefficient significance and quality of model fitness per platform. (B) Euler diagram of DEMs identified in
739 A. (C) Principal component analysis of dual factor DEMs in B clustered by EPs. (D) OBIF summary of
740 molecular drivers of synergy in B-C. (E) Heatmap of expression values of DEMs in B with expression
741 profiles shown per feature (rows). FC, fold change; DEMs, differentially expressed molecules; EPs,
742 expression profiles.

743

744 **Figure EV3. STAT family data and gating strategy for imaging flow cytometry.**

745 (A) Transcription factor activity of STAT subunits 15 min after treatment of human lung epithelial cells
746 with Pam2-ODN. n = 3 samples/condition. (B) Gating strategy used during single cell imaging flow
747 cytometry for simultaneous assessment of all transcriptional subunits.
748
749 **Figure EV4. OBIF improves detection of interaction effects across platforms and factor classes.**
750 (A) Comparative performance of data scaling during interaction analysis at the whole "-ome" level
751 showing overall fitness and significance of two-way ANOVA. (B) Significance level of interaction term
752 between factors detected in A. (C) Comparative performance of statistical methods to detect interaction
753 effects at the individual feature level using a beta-uniform mixture model of interaction p-values. (D)
754 Precision and recall fractions at iDEM selection threshold calculated from C. OBIF, Omics-based
755 interaction framework; ROC, receiver operating characteristic; AUC, area under the curve.

J Pantaleón García, Figure 1

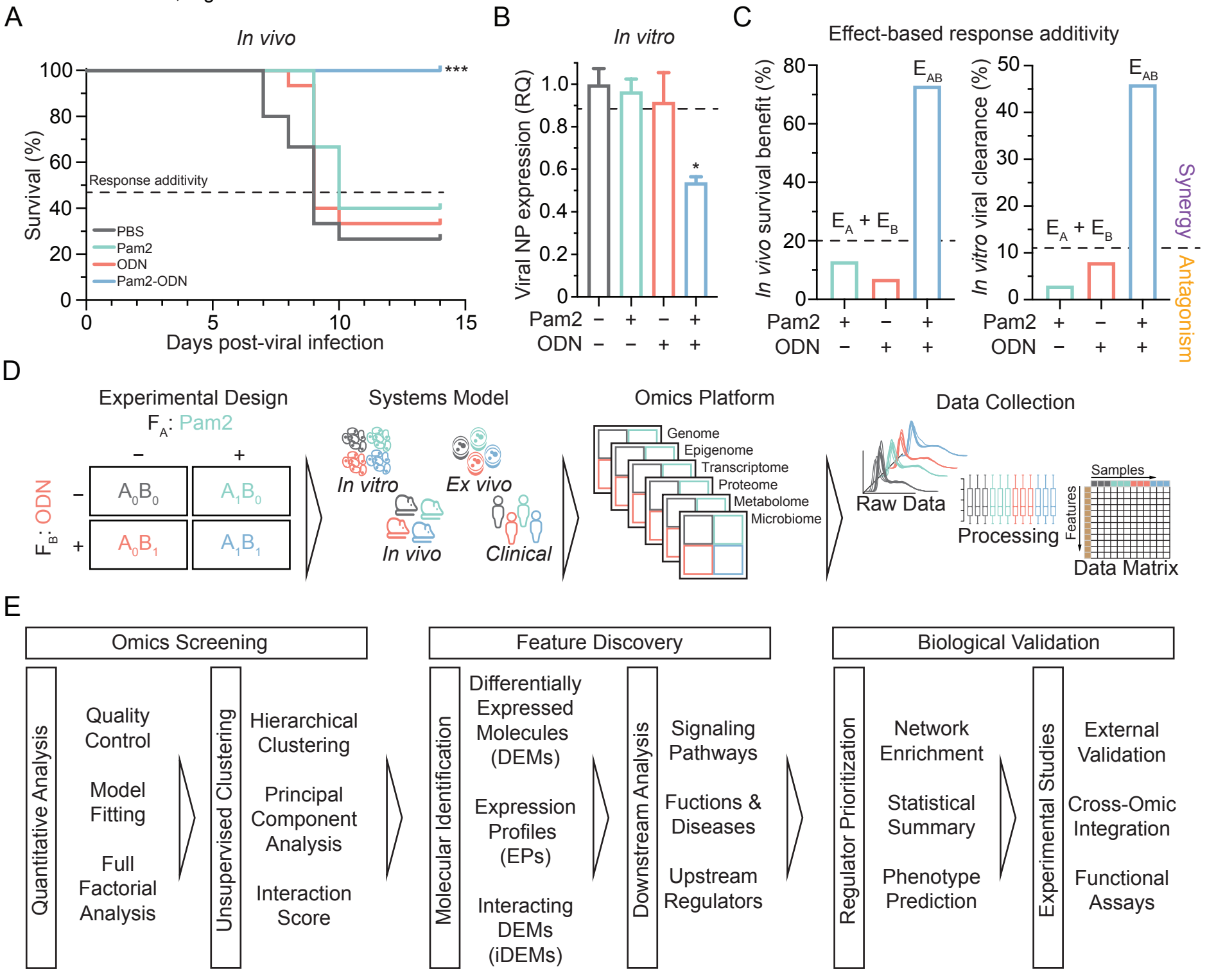

J Pantaleón García, Figure 2

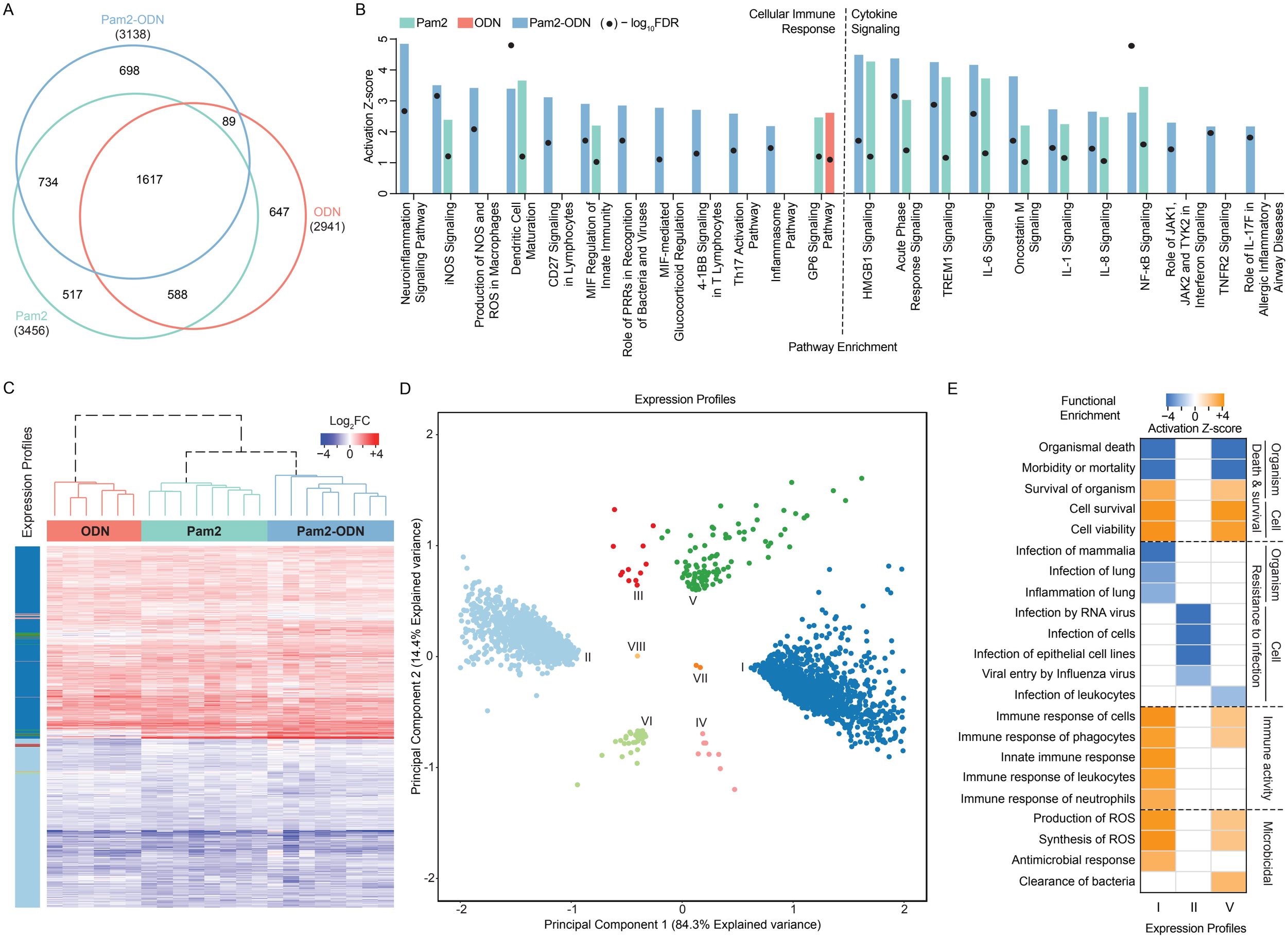

J Pantaleón García, Figure 3

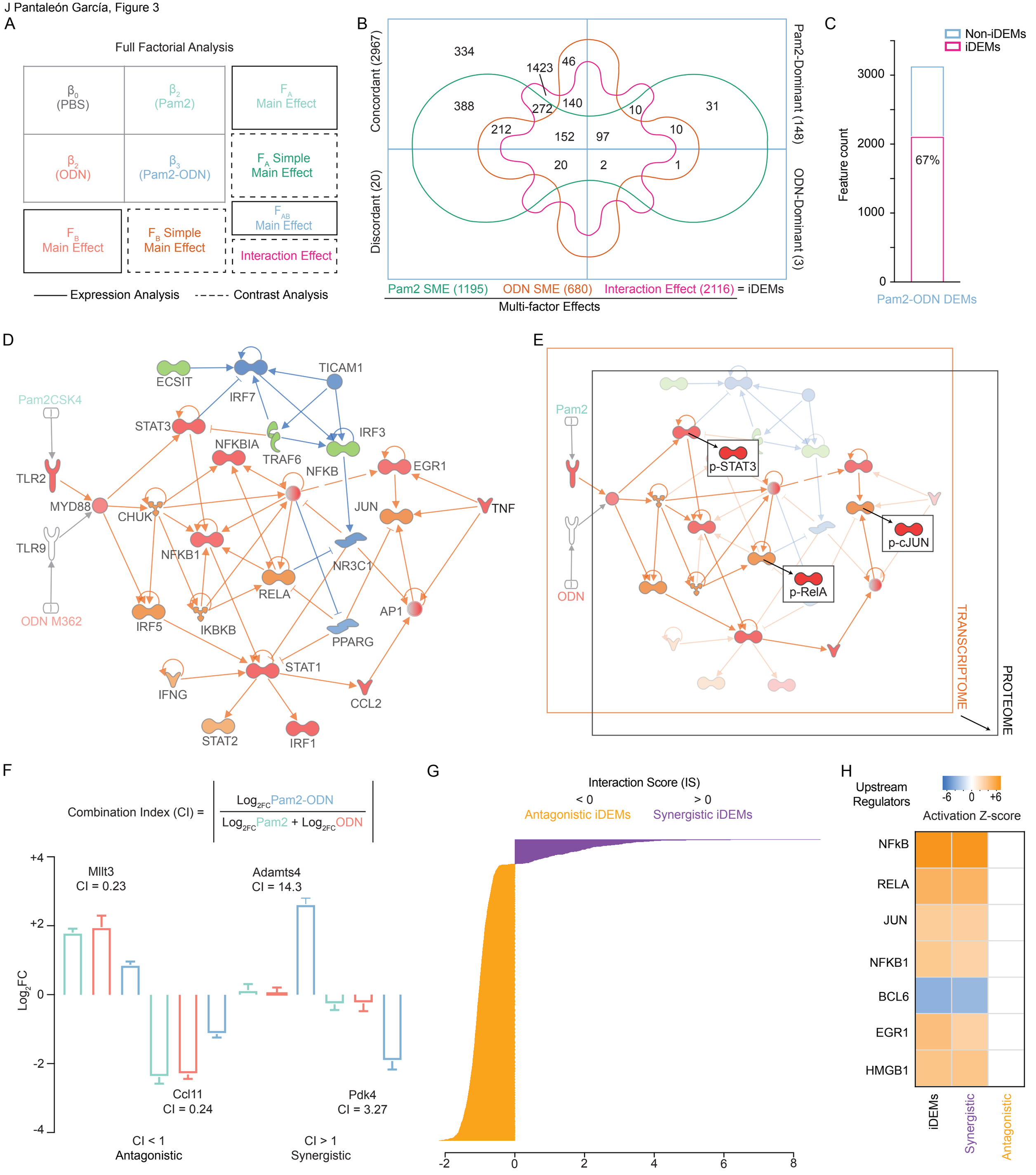

J Pantaleón García, Figure 4

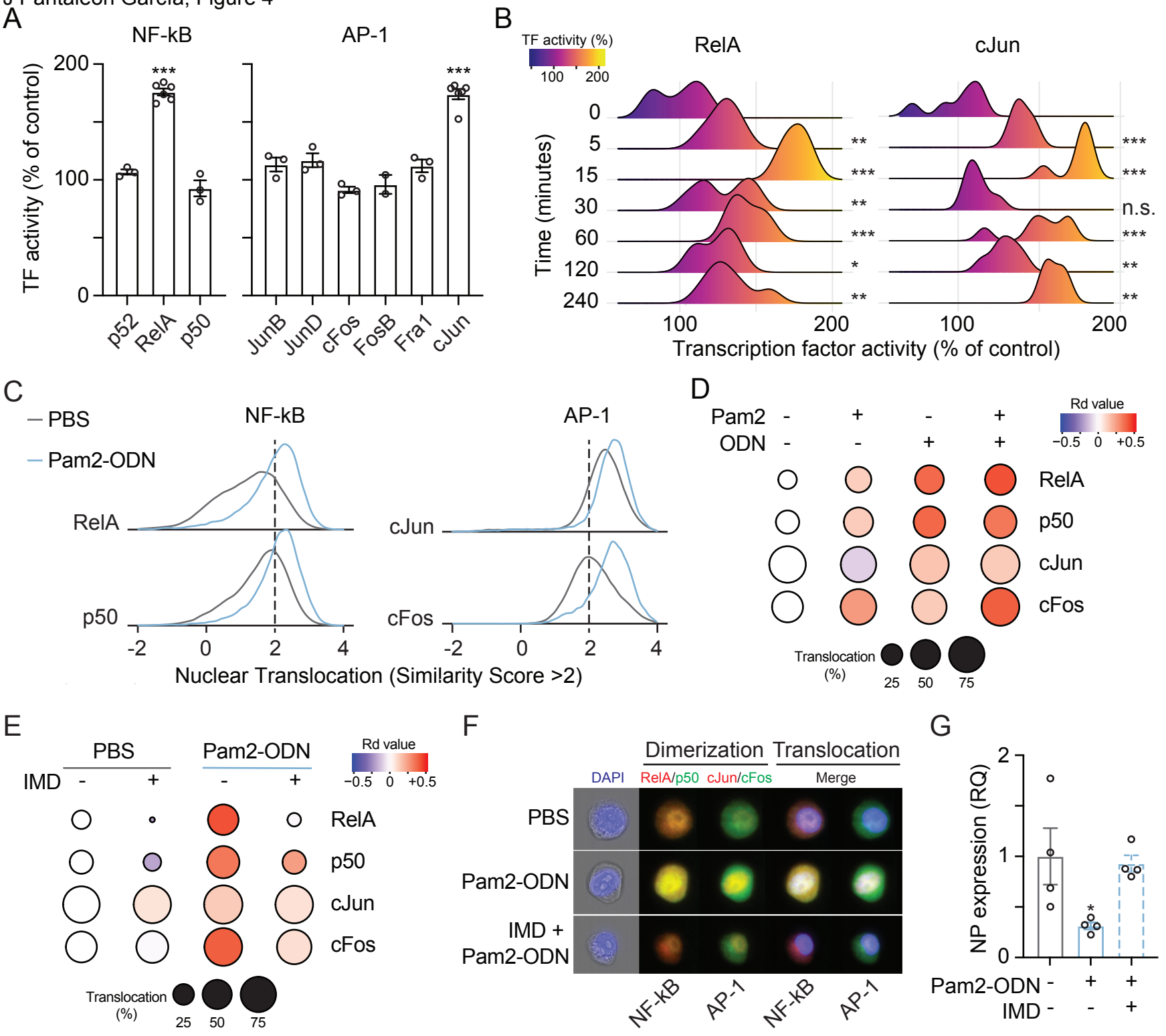

J Pantaleón García, Figure 5

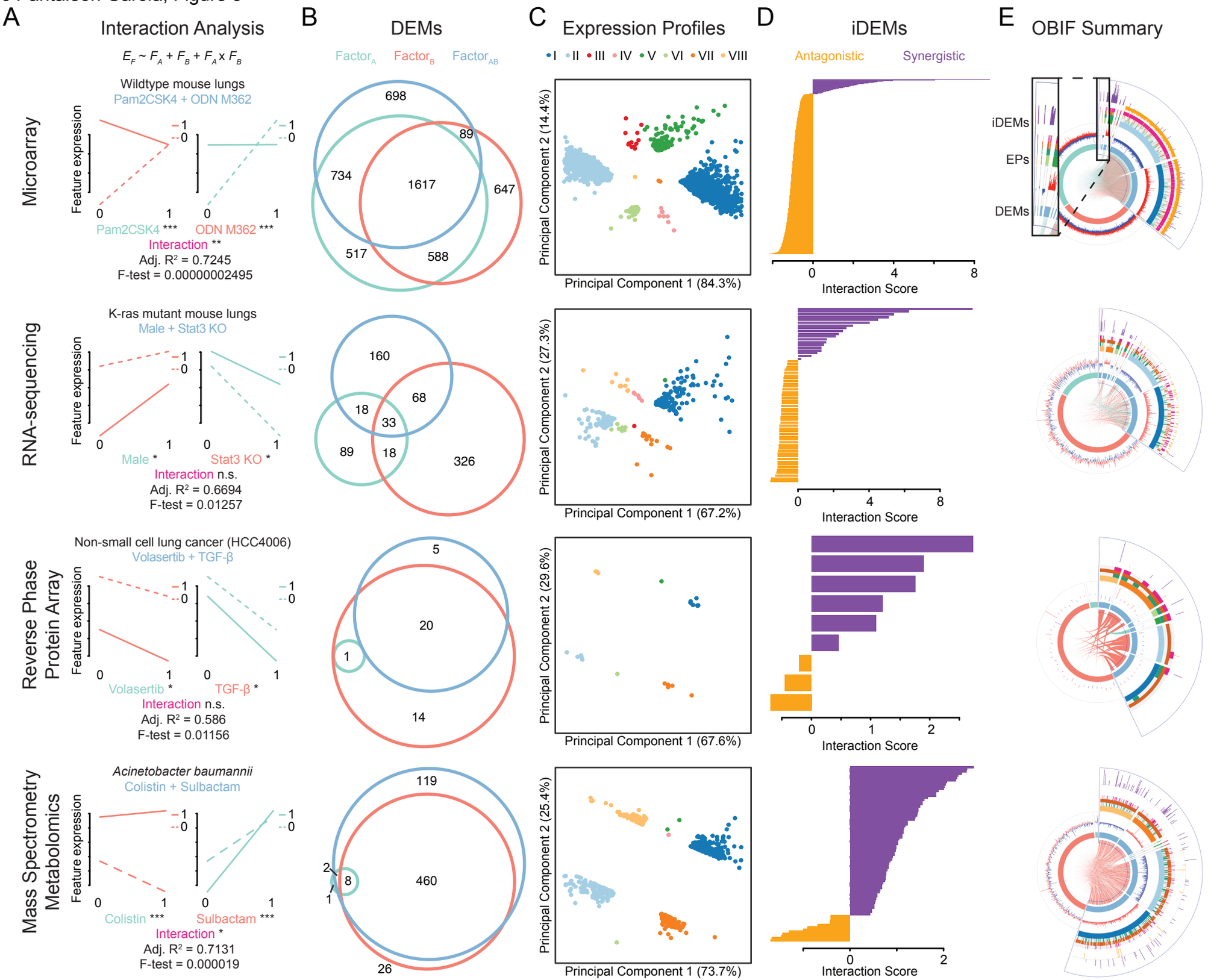

J Pantaleón García, Figure EV1

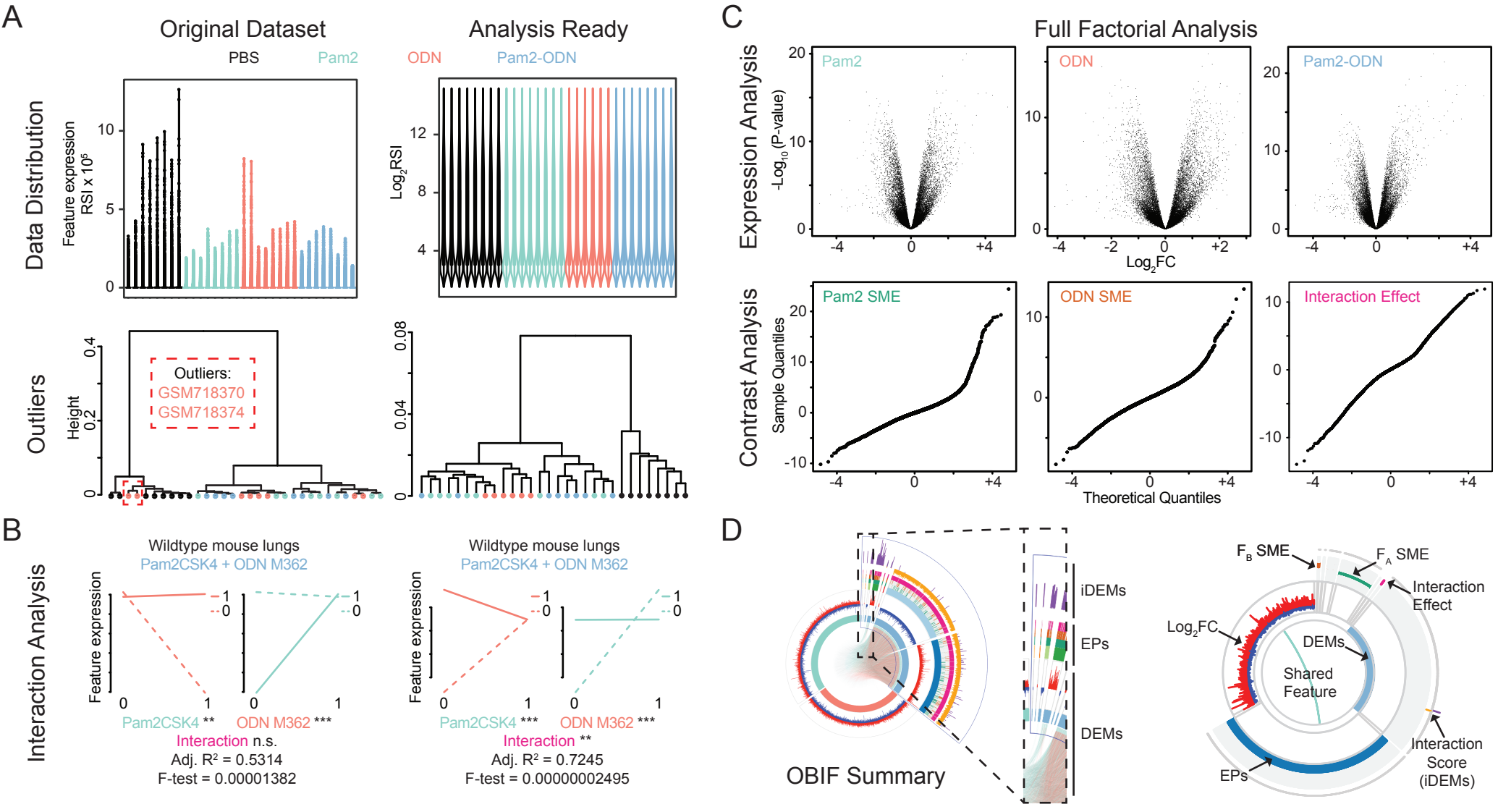

J Pantaleón García, Figure EV2

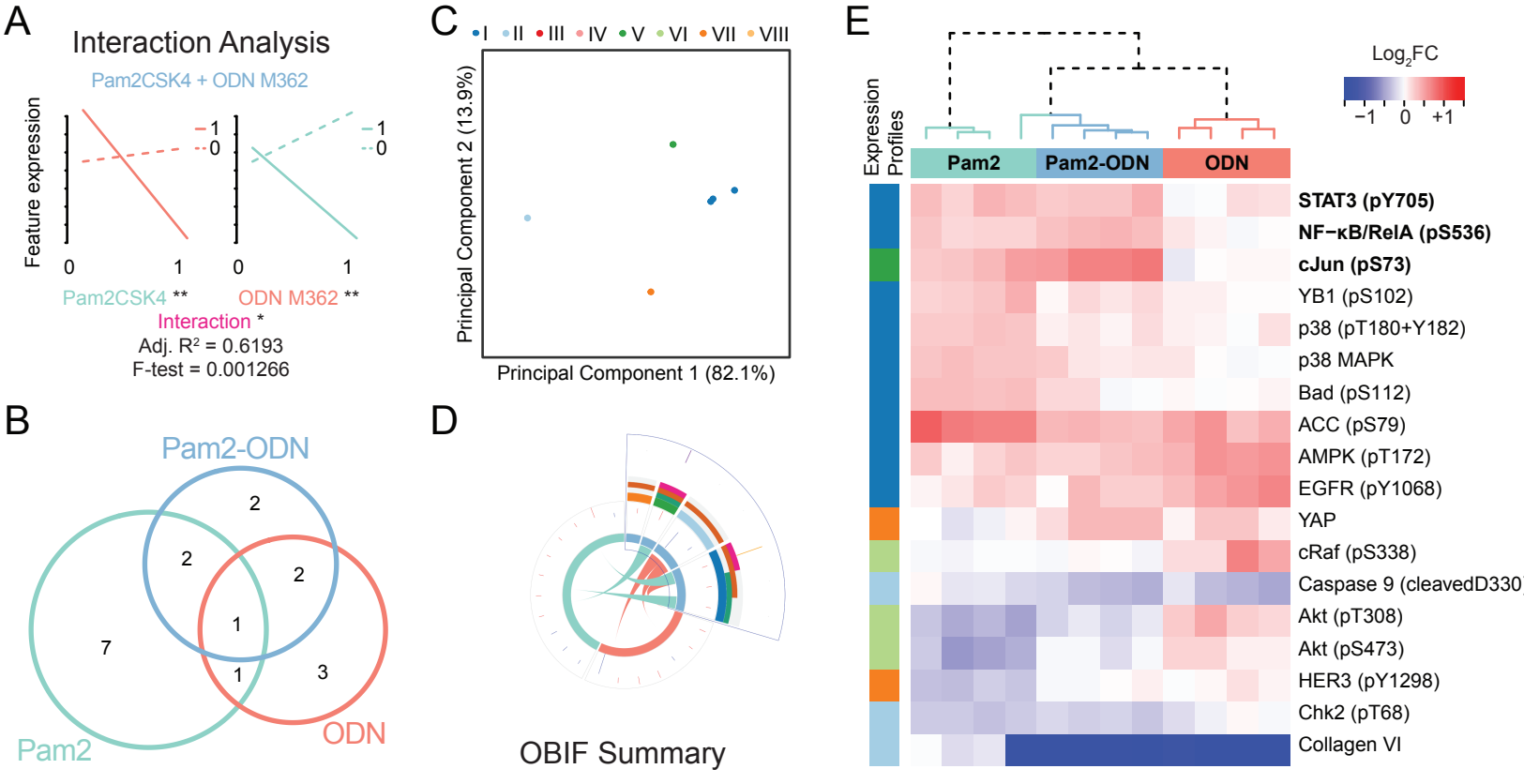

J Pantaleón García, Figure EV3

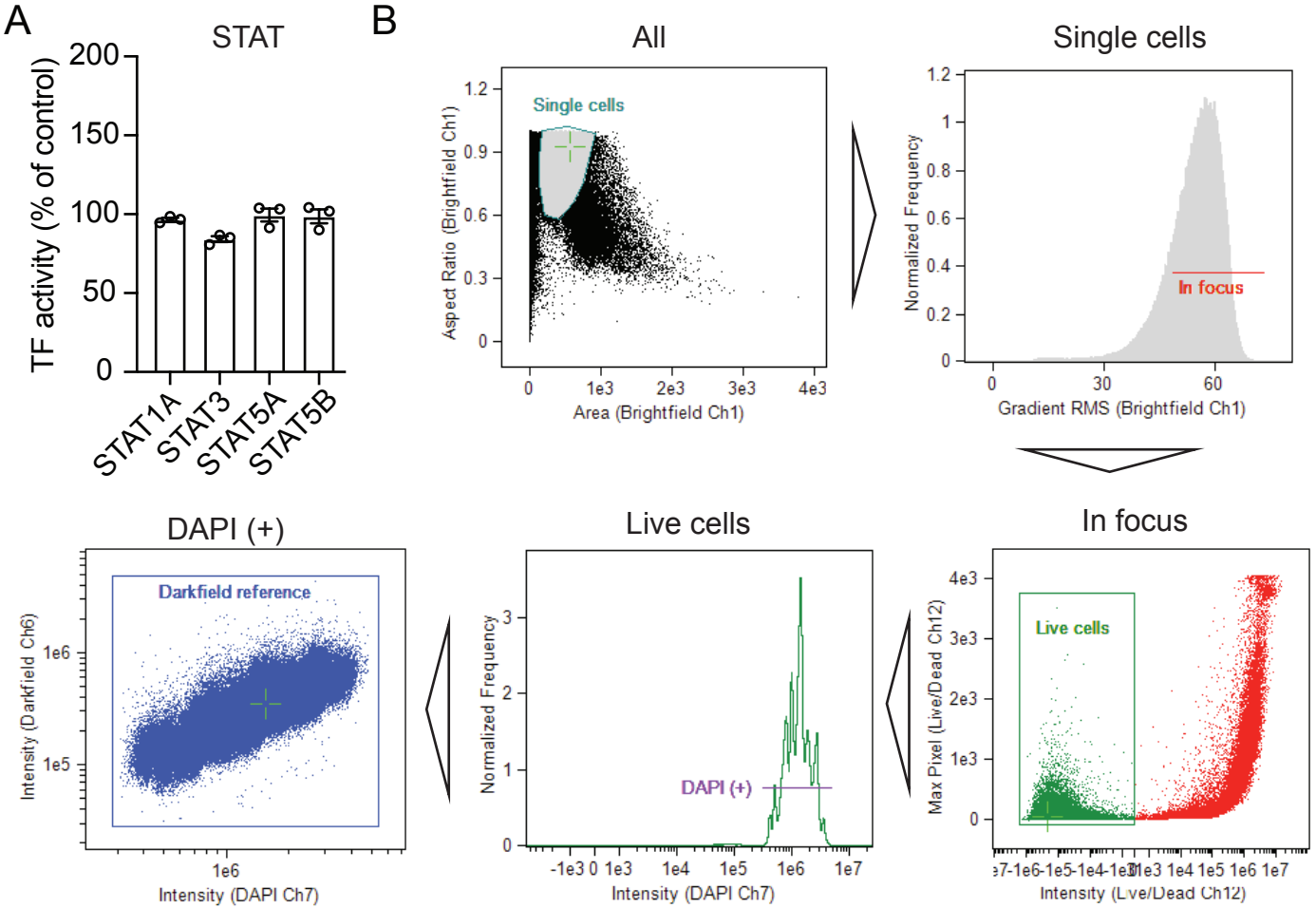
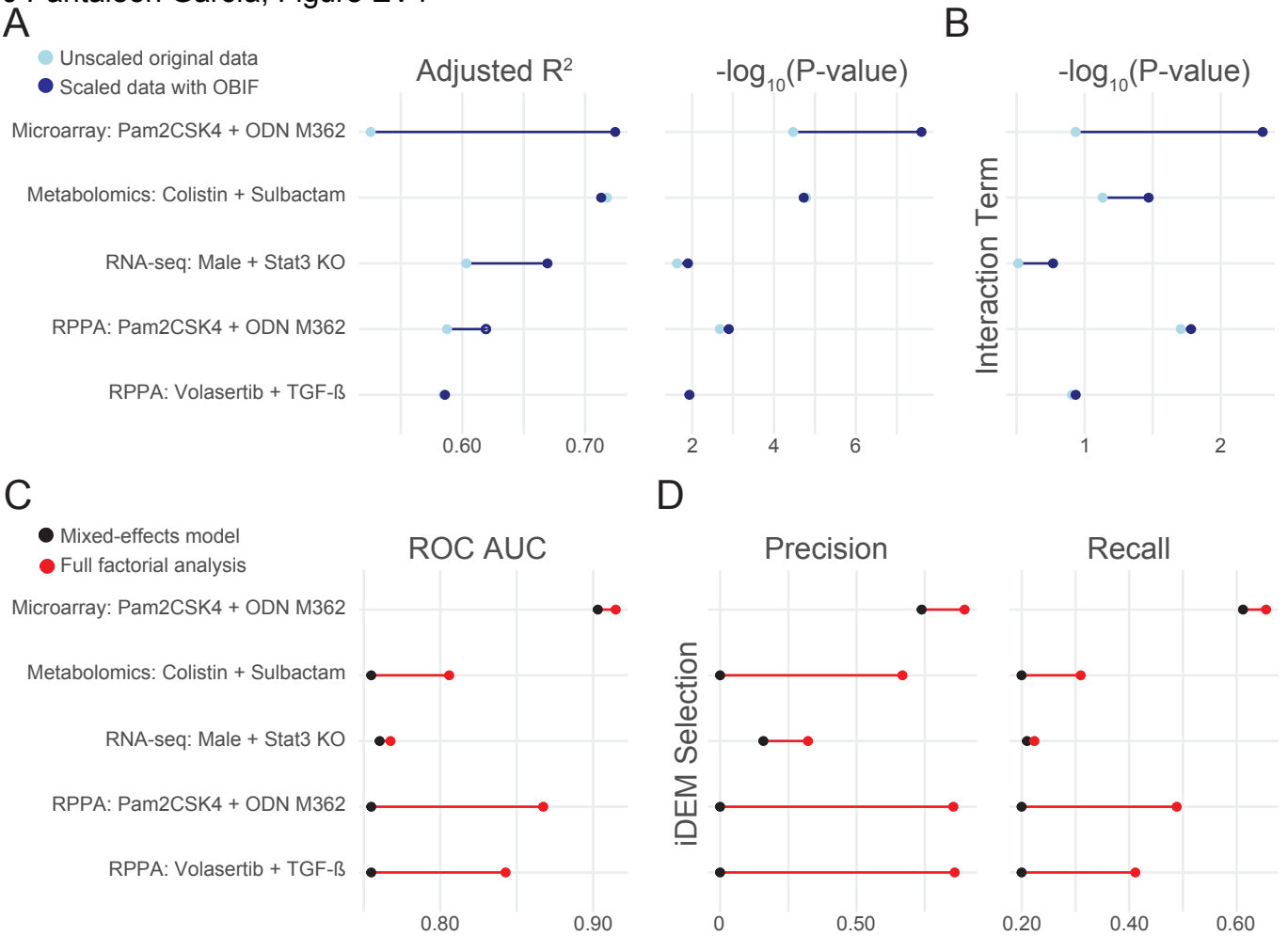
J Pantaleón García, Figure EV4